Vol.67: e24230640, 2024
https://doi.org/10.1590/1678-4324-2024230640
ISSN 1678-4324 Online Edition

BABT
Brazilian Archives of Biology and Technology

Article - Human and Animal Health

Adjuvant-induced Arthritis in the Metatarsophalangeal Joint of Rats: a Stereological Study

Rafael Maciel dos Santos[1]
https://orcid.org/0000-0003-1588-9861

Lucas Castanhola Dias[1,5]
https://orcid.org/0000-0002-9361-9886

Antonio Luiz Boechat[2]
https://orcid.org/0000-0001-5597-7343

Silvânia da Conceição Furtado[3]
https://orcid.org/0000-0003-0065-3119

Aguyda Rayany Cavalcante Barbosa[1]
https://orcid.org/0000-0002-3644-9147

Oscar Tadeu Ferreira da Costa[4*]
https://orcid.org/0000-0003-1550-8969

[1]Universidade Federal do Amazonas, Programa de Pós-Graduação em Imunologia Básica e Aplicada, Manaus, Amazonas, Brasil; [2]Universidade Federal do Amazonas, Departamento de Parasitologia, Manaus, Amazonas, Brasil; [3]Universidade Federal do Amazonas, Departamento de Anatomia, Manaus, Amazonas, Brasil; [4]Universidade Federal do Amazonas, Departamento de Morfologia, Manaus, Amazonas, Brasil;[5]Universidade Federal do Amazonas Instituto Nacional de Pesquisas da Amazônia, Laboratório Temático de Microscopia Ótica e Eletrônica, Manaus, Brasil.

Editor-in-Chief: Paulo Vitor Farago
Associate Editor: Paulo Vitor Farago

Received: 24-Jun-2023; Accepted: 06-Oct-2023

*Correspondence: oscarcostaufam@gmail.com; Tel.: +55-92-98118-8441 (O.T.F.C.).

HIGHLIGHTS

- Rheumatoid arthritis (RA) is a chronic inflammatory autoimmune disease.
- The 5th metatarsophalangeal joint (5MTP joint) are the primary target for RA.
- Stereological analysis provided details of changes induced by chronic inflammation.
- The 5MTP joint is a potential morphological biomarker for RA effects.

Abstract: Small joints are the primary target for rheumatoid arthritis (RA). However, few studies have investigated the quantitative aspects of these changes using a design-unbiased stereological method. Eight male Lewis rats were randomized to either an arthritis group (complete Freund's adjuvant at the base of the tail) or a control group (saline solution). After 28 days the 5th metatarsophalangeal joints (5MTP joint) were decalcified and embedded in methylmethacrylate. The fingers were systematically sectioned perpendicular to the joint cartilage surface to produce 10-12 vertical sections. We quantified the morphological changes in four steps: (i) determination of the Cavalieri volume of joints, (ii) ascertainment of the volume density of tissues, (iii) estimation of the cartilage surface area, and (iv) 3-D counting of chondrocytes and mast cells. Arthritic joints were edematous due to a significant increase in the periarticular region. Synovium volume was inversely related to synovial space. Stereological analysis provided details of changes induced by chronic inflammation, particularly edema, synovial space narrowing, synovitis, mast cell recruitment, bone remodeling, and chondrocyte loss in 5MTP joints. These interrelated pathological changes in chronic inflammation collectively contribute to the progressive joint damage and dysfunction seen in arthritis.

Keywords: Arthritis; Chondrocytes; Mast cell; Synovium; Stereology.

GRAPHICAL ABSTRACT

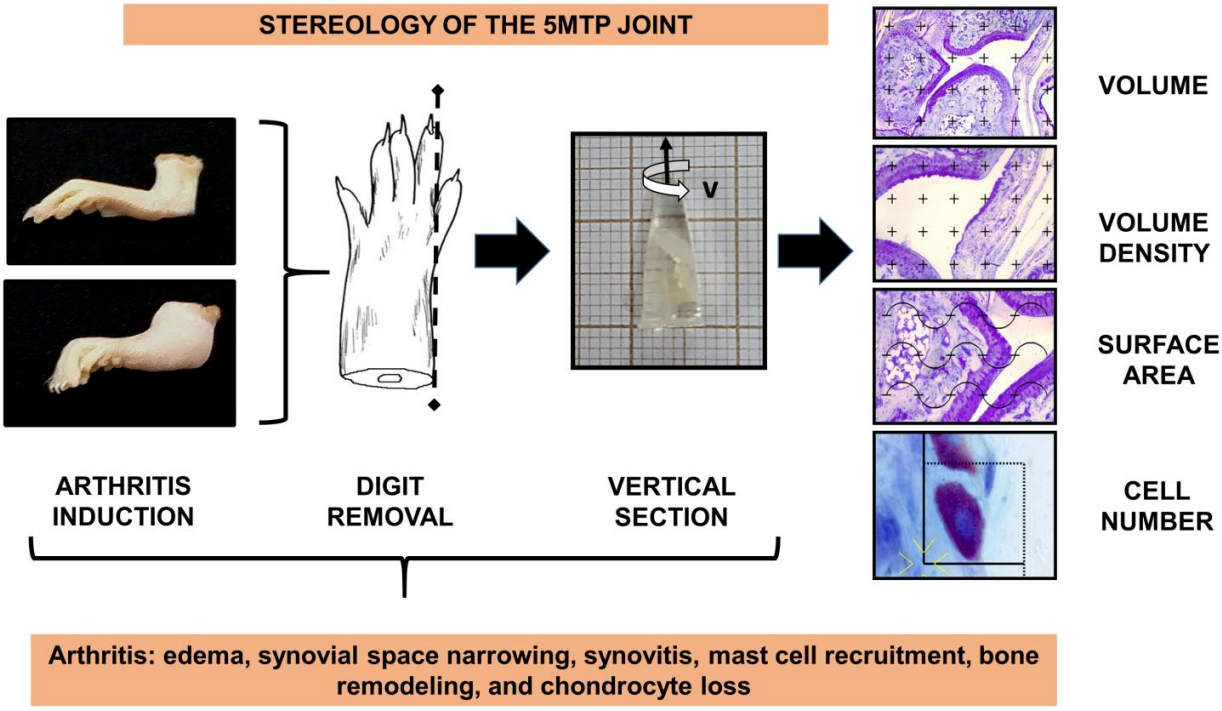

INTRODUCTION

Rheumatoid arthritis (RA) is a chronic inflammatory autoimmune disease of unknown origin and is characterized as one of the most prevalent arthropathies worldwide. The inflammatory process results in increased joint volume and stiffness, causing pain along with systemic symptoms such as fatigue, weight loss, and anemia. Synovitis is the primary factor leading to joint destruction and, if left untreated, can result in severe joint damage and the loss of function. In advanced stages of the disease, symmetrical polyarthritic manifestations can occur, causing deformities and joint degeneration due to bone and cartilage erosion [1, 2].

In RA, the 5th metatarsophalangeal joint (5MTP joint) is particularly affected, showing more evident signs of bone erosion compared with hand joints [3]. The association of these morphological changes with the number of certain cell types, such as mast cells and chondrocytes, can increase knowledge about AR. We know that mast cells population increases in RA and other inflammatory joint diseases [4]. Recent investigations using murine models have shown that mast cell can play a critical role in the perpetuation of this inflammatory process [4-6]. Another cell type that actively participates and is damaged during RA is the chondrocyte [7]. During arthritis, chondrocytes can become activated and produce inflammatory cytokines and enzymes that can break down the extracellular matrix of cartilage. Additionally, chondrocytes may also undergo cell death, leading to further damage to the joint. Therefore, understanding the morphological changes that occur in the joints during arthritis can provide important insights into the pathophysiology of the disease.

Stereology, a quantitative method, provides three-dimensional information about structures from two-dimensional sections. In the context of joint diseases, stereology improves the understanding of diseases, including osteoarthritis and RA [8-13]. Stereological methods can be used to accurately measure the volume, surface area, and the thickness of the cartilage and bone in joint tissues. This can provide valuable information about changes in these tissues during joint diseases, such as the extent of cartilage loss or bone erosion [14]. Additionally, the number, size, and morphology of cells in joint tissues, can be used to quantify changes in inflammatory cells [8]. This can help to identify cellular mechanisms underlying joint disease, such as changes in cell proliferation, differentiation, and cell death. By identifying cellular and structural changes in joint tissues, stereology may also help identify potential targets for the development of new therapies. The aim of the present study was to evaluate the effects of RA on a small joint using modern stereology associated with multivariate analysis to simplify the complexity of datasets and identify hidden patterns or trends.

MATERIAL AND METHODS

Animals, arthritis induction, and study design

Eight male Lewis rats of eight weeks of age (Central Animal Facility from Universidade Federal do Amazonas/UFAM, Brazil) were housed with water and ration ad libitum in a room with controlled temperature, which was set to 22° C, and a light and dark cycle of 12/12 h. The animals were divided into 2 groups, with four animals housed per cage. All experiments were conducted with the approval of the Institutional Ethics Committee on Animal Experimentation. In one group, experimental arthritis was induced in rats weighing an average ± standard error of mean (SEM) of 396 ± 30.89 g by injecting 0.1 mL of a single dose of complete Freund's adjuvant, and 1 µg of the heat-killed *Mycobacterium tuberculosis* strain H37RA (Difco, Detroit, Michigan, USA) into the base of the tail on day 0. The second group of rats was used as a control, and these animals, which weighed 370 ± 13.96 g were injected with an equal volume of saline and maintained under the same conditions as the experimental group. After 28 days, the animals were euthanized by cervical dislocation after intravenous injection of 3 mL of 200 mg/mL stock of sodium pentobarbital (Sigma-Aldrich, USA) in the posterior paw. The 5MTP of the injected posterior paw was excised under a stereomicroscope (Leica EZ4D Digital System, Germany) and kept in buffered formalin solution for at least 48 h at room temperature.

Histological processing

Samples were decalcified, dehydrated, and embedded in hydroxyethyl methacrylate plastic resin (Technovit® 7100, Heraues Külzer, Germany). Before sectioning, the blocks were rotated randomly according to the vertical section protocol [15] (Figure 1a). The total width of each 5MTP joint within the resin block was measured and 10-12 equidistant serial sections 25 µm a part were cut, with the first section being obtained randomly (Figure 1b-c). The appearance and disappearance of the synovial space characterized the first and last section used in this study, respectively. Serial sectioning was done on a microtome (Leica RM2125RT, Germany), and the sequence information of the sections was recorded. The 10 µm thick sections were stained with basic fuchsin and 0.5% toluidine blue. This staining technique allows the detection of mast cells in the synovial capsule by revealing their numerous cytoplasmic metachromatic granules.

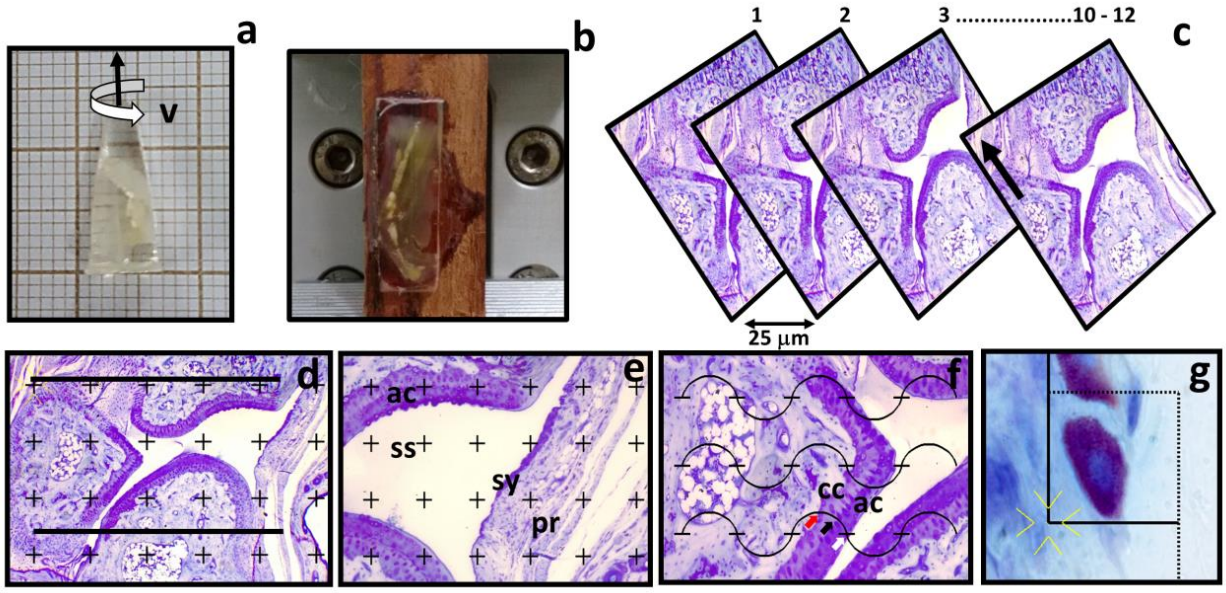

Figure 1. Sampling and stereology. a. A digit embedded in resin is rotated to indicate the vertical orientation (v) of the microtomy. b. Resin block on microtome. c, Serial sections from one digit 25 µm apart. Arrow indicates the vertical direction. d. Section superimposed with a test point system for the determination of Cavalieri volume. At magnification 8, the structures marked in the image are fully visible. The line delimits the area investigated in this study limited by the border with the subchondral cortical bone. e. Test system to estimate the density of 5MTP joint components. f. Test system to estimate cartilage surface area. On the right side of the image, the arrows indicate the intersections counted on each surface. Red arrows = calcified cartilage (cc); black arrows = tidemark; white arrows = articular cartilage (ac). g. Test system containing frames for counting the number of mast cells and chondrocytes. pr, perivascular region; sy, synovium; ss, synovial space.

Stereological analysis

Joint volume

The Cavalieri principle [16] was applied to determine the volume of the 5MTP joints. This technique is based on robust mathematical analysis, which is simple and extremely efficient [17-20]. The joints were photographed (Olympus BX-41 microscope, Japan) in their entirety at a magnification of 8 and overlaid with a counting test system containing crosses generated by Imod (version 4.7/stereology) [21]. Each time the central point of the crosses touched the reference area for the 5MTP joint including the periarticular region, a unit was counted. The evaluated joint area consisted of the limits of the subchondral cortical bone of both the phalangeal and metatarsal sites, and included the sesamoid bone (Figure 1d). The absolute volume of the 5MTP joint was calculated as follows: $(\boldsymbol{mm^3}) = \sum_{i=1}^{m} \boldsymbol{Pi} \times \boldsymbol{T} \times \boldsymbol{a/p}$, where V is the absolute volume of the joint, $\sum_{i=1}^{m} \boldsymbol{Pi}$ is the sum of points hitting the joint, $\boldsymbol{a/p}$ is the area occupied by each central point (11,867 μm^2), and T is the distance between each section, i.e., 25 μm.

Volume density of articular components

The percentage of each component within the 5MTP joint was obtained by the Delesse principle [22]. To obtain this information, the microscopic fields of view used were systematic, uniform, and images were randomly sampled at a magnification of 200. Subsequently, these magnified sections were photographed and superimposed with a counting test system using the procedure outlined earlier to measure the joint volume (Figure 1e). The percentage of volume occupied by each component relative to the reference space (5MTP joint) was calculated as: $\boldsymbol{Vv}\,(\boldsymbol{component, reference\ space}) = \frac{\sum_{i=1}^{m} \boldsymbol{Pcomp}}{\sum_{i=1}^{m} \boldsymbol{Pref}}$, where *Vv* is the volume density of an articular component, $\sum_{i=1}^{m} \boldsymbol{Pcomp}$ is the sum of points hitting each component such as the periarticular region, synovial space, articular cartilage, calcified cartilage, synovium and subchondral cortical bone, and $\sum_{i=1}^{m} \boldsymbol{Pref}$ is the sum of points hitting the reference space [18]. The percentage values obtained for each component were transformed into absolute values when multiplied by the Cavalieri volume of the joint.

Cartilage surface area

The area of any structure can be accessed via the Buffon principle [23], which established that the probability of a line intersecting the edge of a surface is proportional to the surface area of the structure of interest. To estimate the area of the articular and calcified cartilage as well as the tidemark, a counting system using semicircles was superimposed on the images obtained at a magnification of 200, and the intersections between these lines and the cartilage border were counted (Figure 1f). The surface density of the cartilage was obtained as follows: $\boldsymbol{Sv}\left(\boldsymbol{mm^{-1}}\right) = \frac{2\sum_{i=1}^{m} \boldsymbol{I}}{\sum_{i=1}^{m} \boldsymbol{Pi} \times \frac{\boldsymbol{l}}{\boldsymbol{p}}}$, where $\sum_{i=1}^{m} \boldsymbol{I}$ is the number of intersections between the test lines and the cartilage surface, $\frac{\boldsymbol{l}}{\boldsymbol{p}}$ refers to the length of each test point (23.35 μm), and $\sum_{i=1}^{m} \boldsymbol{Pi}$ indicates the total number of points hitting the cartilage tissue.

Number of cells

The theory of counting particles was developed by Wicksell [24] who concluded that there is no relationship between the total number of particles and their two-dimensional count. Therefore, a three-dimensional approach should be employed, as the counting of particles is unbiased in 3-D space. A 3-D quantification according to the Disector principle [25] was used to determine the number of mast cells and chondrocytes in the periarticular region and cartilage, respectively. To do this, a test system containing four lines delimiting a counting frame was employed (Figure 1g). For mast cells and chondrocyte counts, the volume of the Disector was 25,000 and 158,062 μm^3, respectively. The difference in volume occurs due to different dimensions of the two cell types. Nuclear profiles were counted only if they were in the frame or its extensions and did not touch the exclusion lines. The relative number of cells was calculated as follows:

$\boldsymbol{Nv} = \frac{1}{\frac{\boldsymbol{a}}{\boldsymbol{f}} \times \boldsymbol{h}} \times \frac{\sum_{i=1}^{m} \boldsymbol{Q-}}{\sum_{i=1}^{m} \boldsymbol{Pi}}$, where $\frac{\boldsymbol{a}}{\boldsymbol{f}}$ is the area by frame, h (= 10 μm) is the Disector height, $\sum_{i=1}^{m} \boldsymbol{Q}-$ indicates the nuclear counts, and $\sum_{i=1}^{m} \boldsymbol{Pi}$ is the sum of reference points. The total number of mast cells and chondrocytes was obtained by multiplying the relative values by the Cavalieri volume of the periarticular region or cartilage, respectively. All stereological counts were performed by an observer blinded for the group distribution of rats.

Statistical analysis

The statistical program GraphPad Prism 7.0 (GraphPad Software, USA) was used for the statistical and graphical analysis of this study. The data were expressed as mean ± SEM and were tested for normality by the Kolmogorov-Smirnov test. The Student's t-test was used to compare the difference between the mean values of test groups. A 95% confidence interval was established. The stereological data were evaluated for each animal and the variance estimate was determined using the error coefficient as described by [26]. The 15 stereological variables were analyzed via principal component analysis (PCA) to explore the relationship between these variables and the test treatments, and to identify the variables with the greatest influence in the present experimental model. The PCA analysis was performed using the PAST-Paleontological Statistics program, version 3.14 [27].

RESULTS

Morphological and histological analysis of the 5MTP joint

Polyarticular arthritis developed in the hind paws of the adjuvant-injected animals, and the paws were swollen and erythematous compared to the control group (Figure 2a-d). The animals had difficulty walking in their cage and avoided putting their feet on the floor during movement. The tibiotarsal region was edematous. The tendons were hypertrophied and the rats suffered from tenosynovitis (their synovial sheaths were in contact with excess fluid and leukocytes in the extracellular space). Neutrophils were frequently found in the synovium, and were not as common in other regions. Fibrin aggregates were observed in the synovium of the 5MTP joint, which was in close contact with the synovial membrane and the aggregates were also found along the tendon sheaths of the *flexor digitorum profundus*. In the arthritic animals, thickening of the *flexor digitorum profundus* tendon, a reduction in the synovial space of the joints, and an increase in volume of a large part of the connective tissue were observed (Figure 2d).

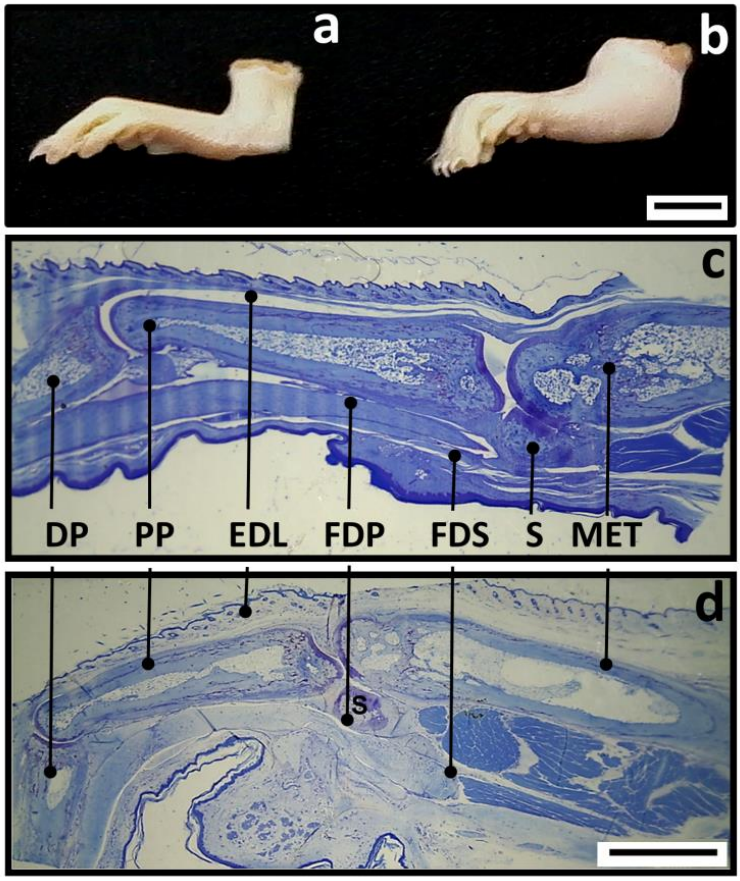

Figure 2. Paws of control animals (a) and arthritic (b). c. Section along the 5th digit revealing the internal organization (control). d. Arthritis. Note the histological changes in the articular and periarticular regions. EDL, *extensor digitorum longus* tendon; FDP, *flexor digitorum profundus* tendon; FDS, *flexor digitorum superficialis* tendon; DP, distal phalanx; PP, proximal phalanx; MET, metatarsus, S, sesamoide bone. a-b, scale bar = 10 mm. c-d, scale bar = 2 mm.

Histological analysis revealed a reduction in synovial space accompanying by subcutaneous edema and synovitis, i.e. synovial membrane hyperplasia (Figure 3). *Pannus* formation was a characteristic of arthritic animals. Lymphocytic foci in the periarticular tissue were observed, and a proliferation of fibroblasts as well, though the latter were not quantified.

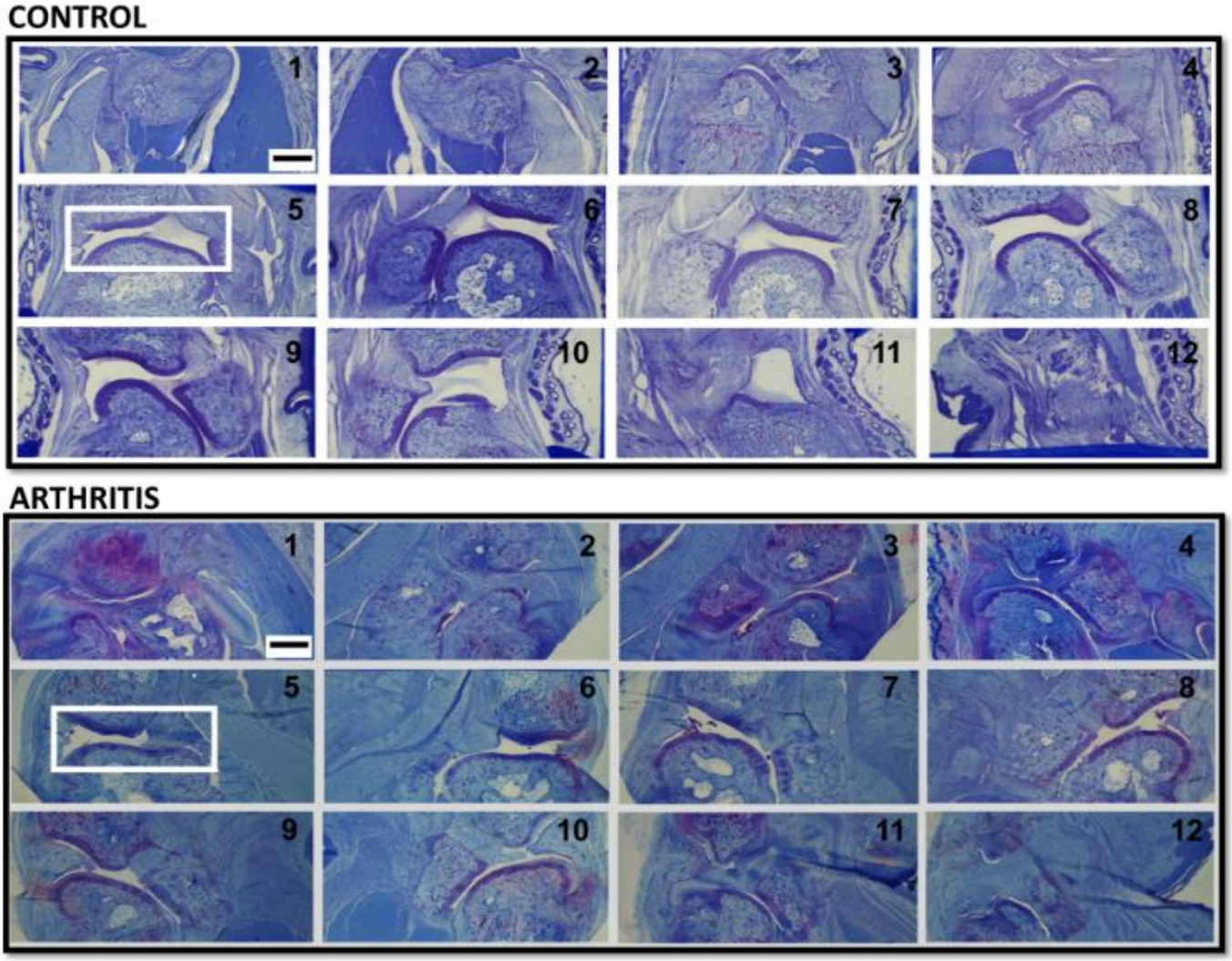

Figure 3. Representative serial sections from 5MTP joint. Note the increased volume of periarticular region and narrowing of the synovial space (white detail in the section 5 in control and arthritic group). Twelve sections were used. Scale bar = 500 μm.

Stereological analysis

The volume of the 5MTP joint was 0.85 mm^3 in the control group and showed a 58% increase to 1.44 mm^3 in the arthritic animals (P = 0.01) (Figure 4a). The major cause of this was the increase in volume by >50% in the periarticular region (P = 0.001) represented by the tendons, ligaments, and capsule (Figure 4a). We did not quantify the extent of the edema; however, it was found to be diffused in the dermis, muscle tissue, and between the tendons. In contrast, the synovial space was the most affected volume component, which was reduced from 0.17 mm^3 in the control group to 0.08 mm^3 in the arthritic animals, i.e. from 20% in the control group to 5.8% in rats with arthritis (P = 0.002; Figure 4b). The volume of the synovium increased from 0.01 mm^3 in the control group to 0.03 mm^3 in the arthritic animals (P = 0.009; Figure 4b). The volume of the cartilage and bone showed a tendency to increase in the arthritic group, but this increase was significant only in the cartilage of the proximal phalanx (P = 0.002) and the subchondral metatarsal bone (P = 0.041; Figure 4c). No significant changes were observed in the sesamoid bone. The surface area of the articular cartilage, tide mark, and calcified cartilage increased in the arthritic group (Figure 4d).

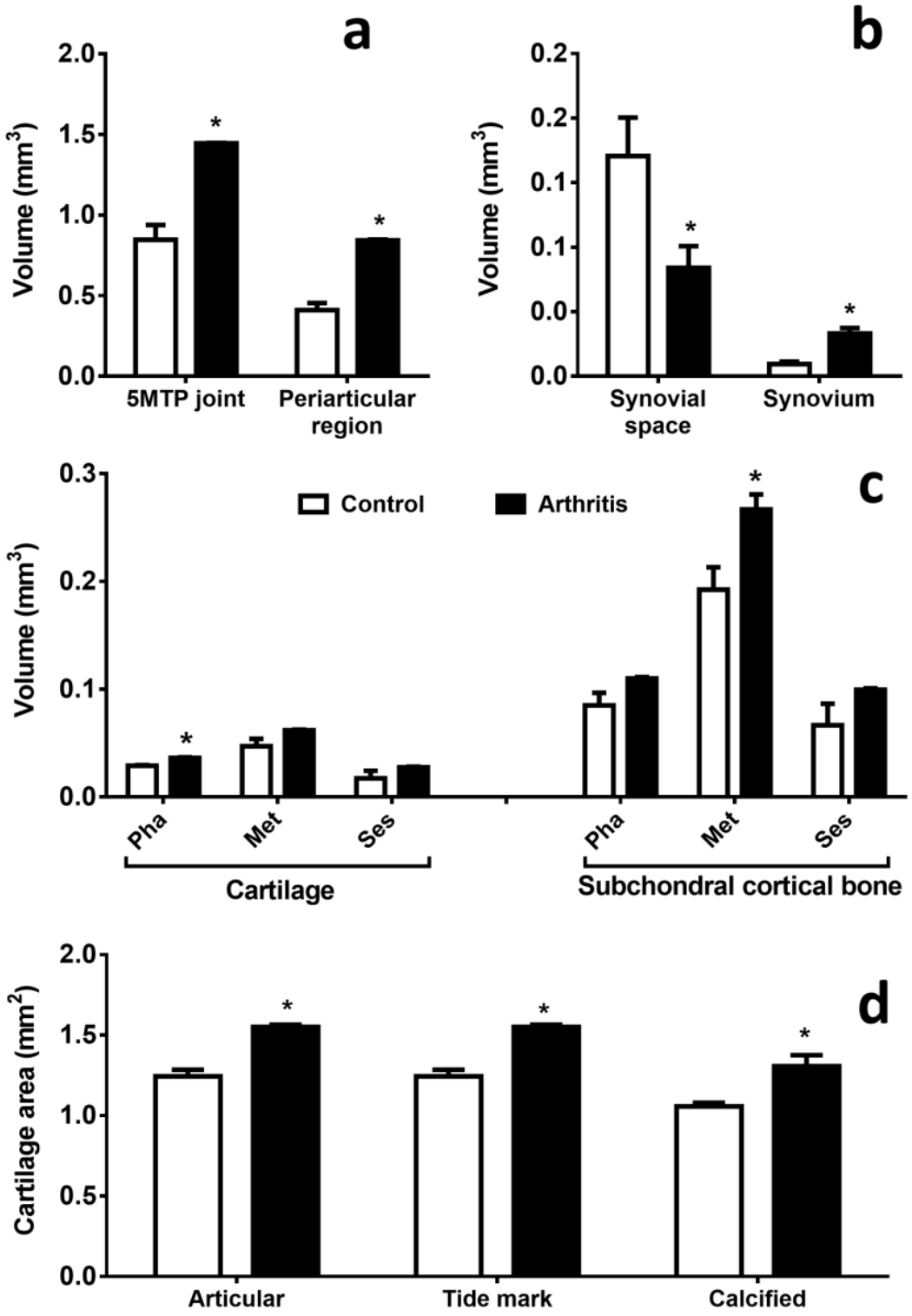

Figure 4. a. Volume of the 5MTP joint and periarticular region. b. Volume of the synovial space and synovium. c. Volume of cartilage and subchondral bone of the phalanx, metatarsus and sesamoid. d. Cartilage surface area. * indicates significant difference in relation to the control ($P < 0.05$). Pha, phalanx; Met, metatarsus; Ses, sesamoid.

The arthritic animals showed a reduction in the number of chondrocytes in the cartilage and significant changes in their morphology and distribution when compared to control group (Figure 5 a-c). In controls, mast cells with metachromatic granules were found near blood vessels. Animals with arthritis had increased numbers of mast cells and many of these cells degranulated (Figure 5 d-f).

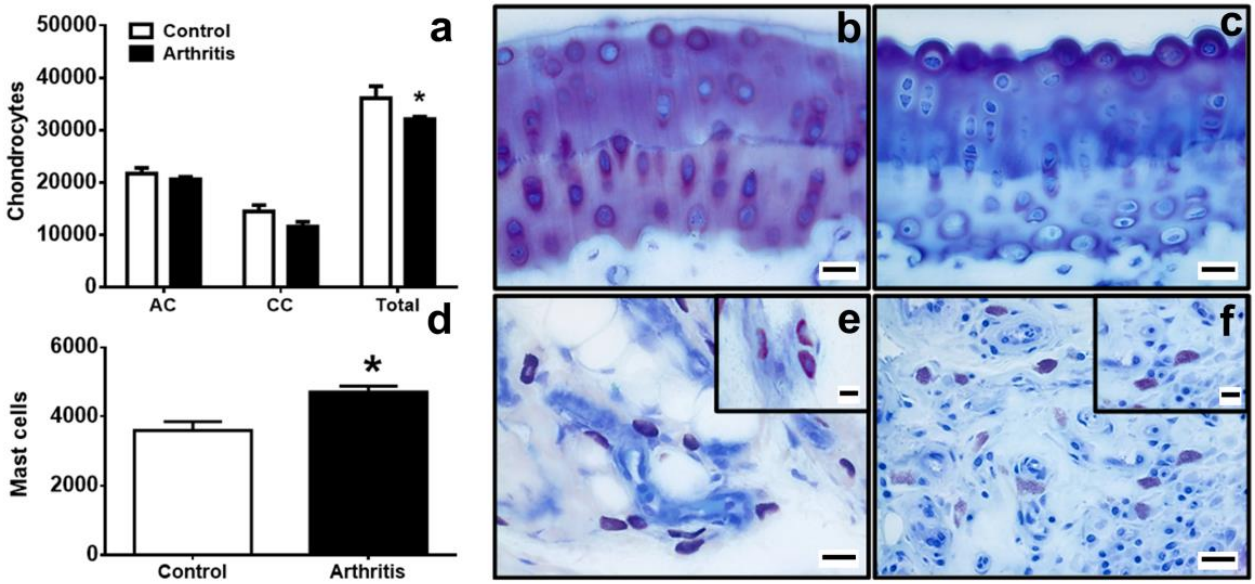

Figure 5. Cell count. a. The number of chondrocytes in the articular (ac) and calcified cartilage (cc). Cartilage morphology of control (b) and arthritics animals (c). Note the changes in chondrocyte morphology and the wavy aspect of the arthritic articular surface. d. The number of mast cells in the periarticular region. Mast cell morphology of control (e) and arthritic animals (f). Note the degranulated state of the mast cells and leukocyte infiltration in arthritic animals compared with control. * indicates significant difference in relation to the control ($P < 0.05$). Scale bar = 20 μm. Details, scale bar = 10 μm.

The PCA analysis revealed that components PC1 (82.41%) and PC2 (8.28%) together accounted for over 90% of the total variance of the original data (Figure 6). The obtained eigenvalues were 12.36 and 1.24 for PC1 and PC2, respectively. The remaining components were not interpreted in this study, as a significant portion of the variance was due to his PC1 and PC2 components. Regarding distribution, control animals showed greater variability (high dispersion), suggesting that they have different characteristics or behaviors. The opposite occurred in arthritis. Relative to PC1, the arthritic animals showed the strongest positive correlations between the volumes of the joint, periarticular region, bone, and cartilage (phalanx, metatarsal, and sesamoid), as well as the synovium, the number of mast cells and chondrocytes, and cartilage area. The volume of the synovial space and the number of chondrocytes showed negative loadings in arthritic animals, and no correlation was found between these parameters. In addition, the volume of the synovial space was inversely correlated with the volume of synovium. The volume of cartilage (except phalanx) and bone were inversely correlated with the number of chondrocytes in arthritic animals.

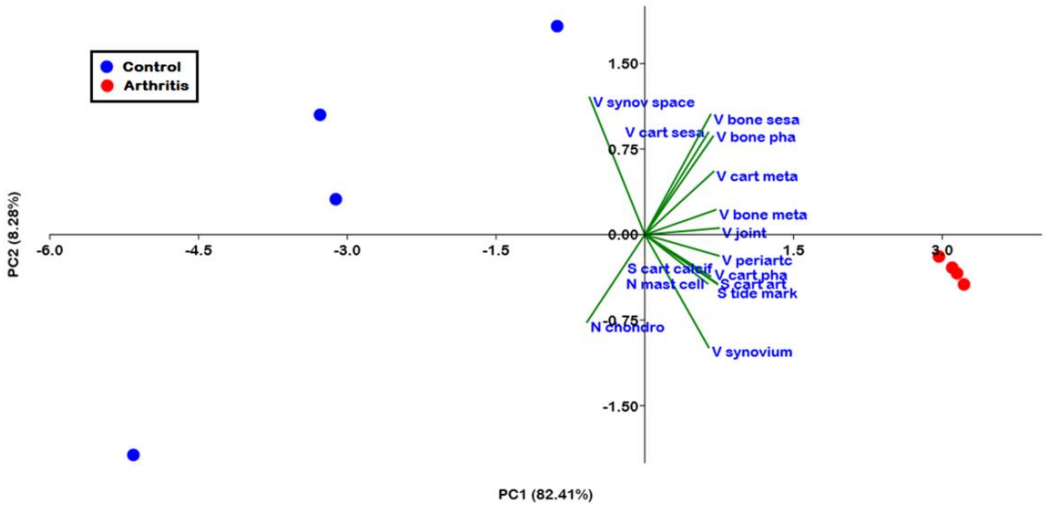

Figure 6. Multivariate analysis representing the projections of the main components (PC) extracted and the loadings of the original data presented as projected lines on the main axes. The contribution of each component to the variability of the data is indicated in parentheses. V, volume, N, number of cells; S, surface area.

The effect caused by the number of sections (effort) on the volume estimation and respective errors (error coefficient) using data from the synovial space of an arthritic animal as example (Figure 7). After the preparation of 12 sections, the plateauing of the curve indicated volume stabilization with the error coefficient below 5%.

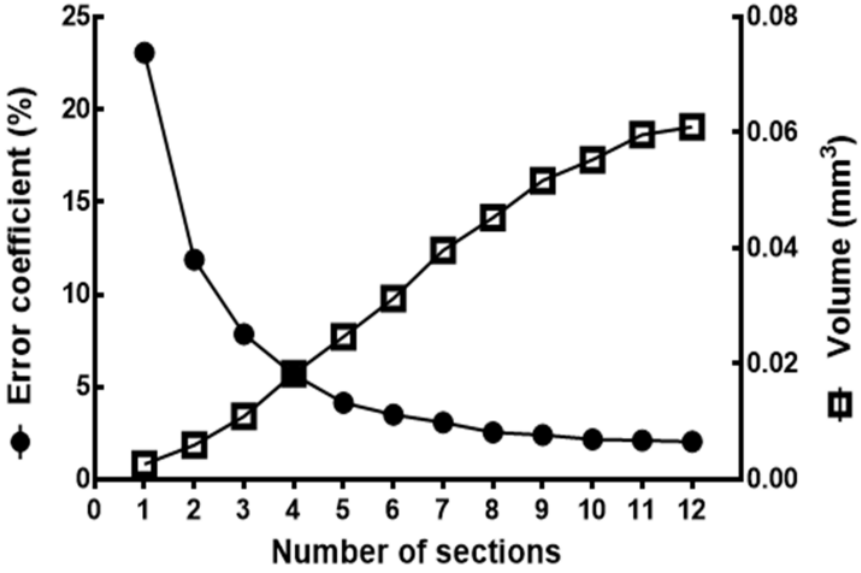

Figure 7. Relationship between the error coefficient, the volume of the synovial space, and the number of histological sections obtained.

DISCUSSION

The present study was conducted to assess the potential of stereology to produce 3D data from serial sections of a small joint, the 5MTP joint, by investigating the effect of collagen-inducing arthritis. Our results demonstrate that arthritis results in edema, inflammation, reduction of synovial space, synovitis, mast cell recruitment, chondrocyte loss, bone remodeling, and changes in cartilage organization. The ease in obtaining this small joint, which is also the most frequently eroded joint in RA, together with the efficiency of histological processing and stereological quantification, make these joints a potential morphological biomarker for the study of experimental arthritis.

Arthritic animals showed a 58% volumetric increase in 5MTP, with over 50% contribution of the periarticular region (Figure 2b e 4a). Edema is a common feature of arthritis in rats induced by experimental methods [28]. The mechanisms underlying paw edema in AIA involve a complex interplay between inflammatory mediators, immune cells, and vascular changes. The net effect of these processes is an increase in paw volume due to the accumulation of fluid and inflammatory cells in the paw tissue [28]. There are no published studies that have used stereology to estimate the volume of the 5MTP joint in rats or any other species. Recently, the volume of the 2MTP joint of Lewis rats was reported by Ureña, de Oliveira [29]. Our data are in agreement with this study. Several studies have used stereology to estimate the volume of other joint components, such as articular cartilage, synovial membrane, and subchondral bone, in various joint models [8, 9, 14]. Among the many advantages of using stereology is its ability to detect minimal morphological differences that may play a relevant role in the pathogenesis of RA. These measurements are crucial for understanding the extent of cartilage loss, bone erosion, and alterations in cellular composition within the joint.

Previous studies have reported hypertrophy of the synovium in RA [30-34]. The synovium is a specialized mesenchymal tissue essential for the full functioning of the joint, but it is the site of a series of pathological processes [2, 35]. Using MRI, Savnik, Bliddal [31] showed that the volume of the synovium of the articular MTP joint (all digits) of arthritic patients ranged from 500 to 6000 mm^3 (mean 100-1,200 mm^3 per joint). This same technique applied to the 5^{th} digit of arthritic patients yielded a synovium volume of 540 mm^3 (around 66% increase in relation to the control) [32]. In our study, the synovium of RA group increased in volume by 33% compared to the control group, a result consistent with the literature. Despite representing a small portion of the joint, the arthritic synovium presents a diverse population of cells, such as macrophages, mast cells, T and B lymphocytes, dendritic cells, PMNs, and synoviocytes [35]. The sites between the *pannus* and cartilage are predominantly occupied by activating macrophage populations and synoviocytes capable of

secreting proteases that destroy the cartilage and bone [36]. There is evidence of a direct positive correlation between synovial surface and articular cartilage in mouse and human joints [36]. A positive correlation between synovium volume and cartilage surface was also demonstrated in our study (Figure 6), supporting the concept of cartilage nutrition dependent on synovial fluid [36]. Furthermore, synovium, mast cells, and chondrocytes showed a high positive correlation, confirming that these sites are directly affected by RA.

The narrowing of the synovial space is a characteristic of RA [35]. In our study, the synovial space represented 20% of the joint region in the control group, and this percentage decreased to 5.8% in the arthritic animals. In a study by Goker, Doughan [37], 85% of patients with arthritis had a decrease in synovial space thickness of the hip joint at a rate of 0.1 mm $year^{-1}$. The decrease in synovial space in RA negatively impacts patients by causing joint stiffness, pain, progressive damage, deformities, impaired tissue nutrition, and an increased risk of complications. From a practical point of view, the determination of synovial space volume is one of the simplest measures in this study, because the region presents no localization difficulties and is clearly limited by the cartilages and synovium. Our study found a strong negative correlation between synovial volume and synovial space. The narrowing of the synovial space is a consequence of *pannus* invasion and reduced synovial fluid secretion [28].

The increased volume of articular cartilage observed in the arthritic animals in the present study (detected only in the phalanx) is of interest, as chondrocytes is the major (but not the only) cell type that produces cartilage matrix [38]. Although highly speculative, the increase in cartilage volume may be related to hydration of this component by excess glycosaminoglycans and proteoglycans. One matrix component with high hydration capacity is hyaluronic acid, which can hold more than 10^3 molecules of water [39]. There is evidence of increased levels of this glycoprotein in RA [40, 41].

Increased cartilage surface area as seen here is not a typical finding in RA (Figure 4d). On the contrary, arthritis results in progressive degradation and loss of cartilage tissue. In general, arthritis is associated with cartilage destruction caused by chronic inflammation, mechanical stress, and biochemical imbalances within the joint. This reduces the cartilage surface area as the disease progresses. Independent of the morphometric method applied, the more folds a surface has, the larger its surface will be. Surface folds or erosion are detected by stereology as increases in surface area due to the increase in the number of intersections of these surfaces with lines of the counting system [15]. These ripples were notably observed in the articular cartilage of arthritic animals and explained the increased surface area (Figure 5e-f).

Arthritis reduces the total number of chondrocytes in cartilage (Figure 5a). The death of chondrocytes in the cartilage is a key feature of cartilage degradation, and there are several mechanisms that contribute to its death in arthritis [28]. Apoptosis is a very common way to eliminate cells by a regulated program, and previous studies have shown that chondrocyte death occurs by this pathway [42, 43]. Although we did not analyze cell death in this study, previous research has shown that chondrocyte death may have several implications for the pathogenesis of arthritis. The cartilage is an avascular structure and chondrocytes are contained in its lacunae, which are surrounded by territorial and interterritorial matrix. As there are no mononuclear phagocytes in cartilage, the resulting apoptotic corpuscles cannot be removed from the matrix by phagocytic cells, resulting in secondary necrosis in the extracellular environment, perpetuating the inflammatory process [42].

In our study, we found increased subchondral bone volume in the metatarsals of animals with arthritis (Figure 4c). This phenomenon is known as subchondral bone sclerosis or subchondral bone thickening [44]. The increase in subchondral bone volume in arthritis is thought to be a compensatory response to the ongoing damage and degradation of cartilage. It is believed to be influenced by a complex interplay of mechanical, cellular, and biochemical factors. In a study by Pearson [45], the appearance of fibrous ankylosis occurred on the 45th day after the onset of RA induction in the rat MTP joint, although bone ankylosis was detected on the 30th day. In our study, the rats were euthanized on the 28th day after arthritis induction, and therefore were in the process of bone remodeling. Moreover, our study agrees with Keller, Thomsen [12] who showed, through stereology, that bone remodeling and erosion in tarsal of SKG mice (a model of autoimmune polyarthritis) is a simultaneous process.

An important point in our study is the stereological analysis of the metapodiophalangeal sesamoid bone, whose morphometric information is scarce in the literature. The sesamoids appear as small oval bones adjacent to the joint formed within a continuous bundle of regular dense connective tissue [46, 47]. Its surfaces are covered with cartilage and are intimate with the synovial space. Sesamoids protect tendons from damage and amplify the efficiency of associated muscles by regulating pressure and reducing friction on them, and may undergo reabsorption of their cartilaginous surface and destruction in RA [48]. In our study, the subchondral region of the sesamoid and its articular cartilage showed no change in volume, suggesting that remodeling may occur at a later stage of the inflammatory process.

Animals with arthritis had higher numbers of mast cells, most of which were degranulated (Figure 5d-f). Mast cells have been recognized as important mediators of allergic manifestations; however, recent research has shown that their role goes far beyond immune responses. In a study by Lee, Friend [49], animals deficient in mast cells were completely resistant to RA induction. Mast cells express surface receptors for IgG, complement, PAMPs, and are capable of phagocytosis and presentation of antigens [5]. According to these studies, in the absence of inflammation, mast cells of the synovial membrane represent a population of about 3%, and this number rises to 5% in RA. Mast cells are present throughout the subsynovial and subepithelial regions, with aggregates in the *pannus* [5]. In the initial phase of RA, mast cells are potential mediators of increased vascular permeability and cause induction of endothelial expression of adhesion molecules as well as recruitment and activation of resident leukocytes and macrophages. In chronic synovitis, mast cells participate directly in the activation of fibroblasts, recruitment of macrophages, angiogenesis, the formation of *pannus*, induction of metalloproteinase production, and destruction of the joint [5, 50, 51].

In addition to the quantitative information presented in this study, stereology allows us to measure the errors obtained in our analysis. This error is caused by two main factors: the number of counting events (points/intercepts) and the number of serial sections. As highlighted in our analysis, the impact of the number of sections has a direct influence on the precision (Figure 7). For smaller joints, we recommend using a maximum of 12 serial sections, as this number corresponds to volume measurement stabilization with an error coefficient of less than 5%. Increasing the number of sections would decrease the efficiency of the stereological method, and have little effect on the error [52]. During the microtomy, we recommend that the appearance of the synovial space in the initial microtome sections should be detected, and subsequently, equidistant serial sections around ~ 25 μm should be processed.

The current article demonstrated the potential use of a small joint as a morphological biomarker for RA effects. The stereological analysis revealed details of the changes promoted by chronic inflammation, in particular edema, reduction of synovial space, synovitis, mast cell recruitment, bone remodeling, and changes to the cartilage of the 5MTP joint. Overall, these interconnected pathological changes in chronic inflammation contribute to the progressive joint damage and functional impairment observed in arthritis. Understanding the mechanisms underlying these processes is essential for developing of targeted therapies aimed at alleviating symptoms, slowing disease progression, and preserving joint function.

Funding: This research was funded by CNPq, CAPES and POSGRAD FAPEAM (Fundação de Amparo à Pesquisa do Estado do Amazonas).
Acknowledgments: The authors are grateful to Erilene Carmo dos Santos (UFAM) for her invaluable help with the histotechnological processing.
Conflicts of Interest: The authors declare no conflicts of interest concerning this article's research, authorship, and publication.

REFERENCES

1. Ralphs J, Benjamin M. The joint capsule: structure, composition, ageing and disease. J Anat. 1994;184(Pt 3):503.
2. O'Connell JX. Pathology of the synovium. Am J Clin Pathol. 2000;114(5):773-84.
3. Hulsmans HM, Jacobs JW, Van Der Heijde DM, Van Albada-Kuipers GA, Schenk Y, Bijlsma JW. The course of radiologic damage during the first six years of rheumatoid arthritis. Arthritis Rheum. 2000;43(9):1927-40.
4. Rivellese F, Rossi FW, Galdiero MR, Pitzalis C, de Paulis A. Mast Cells in Early Rheumatoid Arthritis. Int J Mol Sci. 2019;20(8):2040.
5. Nigrovic PA, Lee DM. Mast cells in inflammatory arthritis. Arthrit Res Ther. 2005;7(1):1.
6. Min HK, Kim K-W, Lee S-H, Kim H-R. Roles of mast cells in rheumatoid arthritis. Korean J Intern Med. 2020;35(1):12.
7. Tseng C-C, Chen Y-J, Chang W-A, Tsai W-C, Ou T-T, Wu C-C, et al. Dual Role of Chondrocytes in Rheumatoid Arthritis: The Chicken and the Egg. Int J Mol Sci. 2020;21(3):1071.
8. Artacho-Pérula E, Roldéan-Villa Lobos R, Collantes-Estévez E, López-Beltréan A. Stereological analysis of the synovial membrane in rheumatic disorders: diagnostic value of volume-weighted mean nuclear volume estimation. Histopathology. 1994;25(4):357-63.
9. Hunziker EB. Cartilage histomorphometry. Arthritis Research: Springer; 2007. p. 147-66.
10. Keller KK, Andersen IT, Andersen JB, Hahn U, Stengaard-Pedersen K, Hauge E, et al. Improving efficiency in stereology: a study applying the proportionator and the autodisector on virtual slides. J Microsc. 2013;251(1):68-76.
11. Keller KK, Stengaard-Pedersen K, Dagnæs-Hansen F, Nyengaard JR, Sakaguchi S, Hauge EM. Histological changes in chronic autoimmune SKG-arthritis evaluated by quantitative three-dimensional stereological estimators. Clin Exp Rheumatol. 2010;29(3):536-43.

12. Keller KK, Thomsen JS, Stengaard-Pedersen K, Dagnæs-Hansen F, Nyengaard JR, Hauge E-M. Bone formation and resorption are both increased in experimental autoimmune arthritis. PloS One. 2012;v. 7(n. 12):p. e53034.
13. Wang SX, Arsenault L, Hunziker EB. Stereologic analysis of tibial-plateau cartilage and femoral cancellous bone in guinea pigs with spontaneous osteoarthritis. Clin Orthop Relat Res. 2011;469(10):2796-805.
14. Barck KH, Lee WP, Diehl LJ, Ross J, Gribling P, Zhang Y, et al. Quantification of cortical bone loss and repair for therapeutic evaluation in collagen-induced arthritis, by micro–computed tomography and automated image analysis. Arthritis Rheum. 2004;50(10):3377-86.
15. Baddeley A, Gundersen H-JG, Cruz-Orive LM. Estimation of surface area from vertical sections. J Microsc. 1986;142(3):259-76.
16. Cavalieri B. Geometria indivisibilibus continuorum nova quadam ratione promota. Bologna. First edition Bologna. 1635;1635.
17. Gundersen H, Bendtsen TF, Korbo L, Marcussen N, Møller A, Nielsen K, et al. Some new, simple and efficient stereological methods and their use in pathological research and diagnosis. APMIS. 1988;96(1-6):379-94.
18. Howard CV, Reed MG. Unbiased stereology: three-dimensional measurement in microscopy. 2nd ed. New York, Berlin, Heidelberg: Springer-Verlag; 2005.
19. Mouton PR. Unbiased stereology: a concise guide. 1. ed. Baltimore, Maryland: The Johns Hopkins University Press; 2011.
20. Weibel ER. Stereological methods: Academic Press London; 1980.
21. Kremer JR, Mastronarde DN, McIntosh JR. Computer visualization of three-dimensional image data using IMOD. J Struct Biol. 1996;116(1):71-6.
22. Delesse AEOJ. Procédé mécanique pour déterminer la composition des roches: F. Savy; 1866.
23. Buffon GLL, Comte de Essai d'arithmétique morale. In Supplément à l´Historie Naturalle.1777. 103 p. p.
24. Wicksell SD. The corpuscle problem: a mathematical study of a biometric problem. Biometrika. 1925:84-99.
25. Sterio D. The unbiased estimation of number and sizes of arbitrary particles using the disector. J Microsc. 1984;134(2):127-36.
26. Cruz-Orive LM. Precision of Cavalieri sections and slices with local errors. J Microsc. 1999;193(3):182-98.
27. Hammer Ø, Harper D, Ryan P. Paleontological statistics software: package for education and data analysis. Palaeontol Electron. 2001(4).
28. Firestein GS, Budd R, Gabriel SE, O'Dell JR, McInnes IB. Kelley's Textbook of Rheumatology: Expert Consult Premium Edition: Enhanced Online Features: Elsevier Health Sciences; 2012.
29. Ureña NM, de Oliveira CP, Guterres SS, Pohlmann AR, da Costa OTF, Boechat AL. The Anti-Arthritic Activity of Diclofenac Lipid-Core Nanocapsules: Stereological Analysis Showing More Protection of Deep Joint Components. Molecules. 2023;28(13):5219.
30. Landewé R, Smolen JS, Florentinus S, Chen S, Guérette B, van der Heijde D. Existing joint erosions increase the risk of joint space narrowing independently of clinical synovitis in patients with early rheumatoid arthritis. Arthrit Res Ther. 2015;17(1):133.
31. Savnik A, Bliddal H, Nyengaard JR, Thomsen HS. MRI of the arthritic finger joints: synovial membrane volume determination, a manual vs a stereologic method. Eur Radiol. 2002;12(1):94-8.
32. Klarlund M, Ostergaard M, Lorenzen I. Finger joint synovitis in rheumatoid arthritis: quantitative assessment by magnetic resonance imaging. Rheumatology. 1999;38(1):66-72.
33. Kristensen KD, Stoustrup P, Küseler A, Pedersen TK, Nyengaard JR, Hauge EM, et al. Quantitative histological changes of repeated antigen-induced arthritis in the temporomandibular joints of rabbits treated with intra-articular corticosteroid. J Oral Pathol Med. 2008;37(7):437-44.
34. Hodgson R, O'Connor P, Moots R. MRI of rheumatoid arthritis—image quantitation for the assessment of disease activity, progression and response to therapy. Rheumatology. 2008;47(1):13-21.
35. Firestein GS, McInnes IB. Immunopathogenesis of rheumatoid arthritis. Immunity. 2017;46(2):183-96.
36. Hewitt KM, Stringer MD. Correlation between the surface area of synovial membrane and the surface area of articular cartilage in synovial joints of the mouse and human. Surg Radiol Anat. 2008;30(8):645-51.
37. Goker B, Doughan AM, Schnitzer TJ, Block JA. Quantification of progressive joint space narrowing in osteoarthritis of the hip: longitudinal analysis of the contralateral hip after total hip arthroplasty. Arthritis Rheum. 2000;43(5):988-94.
38. Roughley PJ. Articular cartilage and changes in arthritis: noncollagenous proteins and proteoglycans in the extracellular matrix of cartilage. Arthrit Res Ther. 2001;3(6):1-6.
39. Alberts B, Johnson A, Lewis J, Morgan D, Raff M, Roberts K, et al. Molecular biology of the cell: WW Norton & Company; 2017.
40. Poole AR, Witter J, Roberts N, Piccolo F, Brandt R, Paquin J, et al. Inflammation and cartilage metabolism in rheumatoid arthritis. Studies of the blood markers hyaluronic acid, orosomucoid, and keratan sulfate. Arthritis Rheum. 1990;33(6):790-9.
41. Goldberg RL, Huff JP, Lenz ME, Glickman P, Katz R, Thonar EJ. Elevated plasma levels of hyaluronate in patients with osteoarthritis and rheumatoid arthritis. Arthritis Rheum. 1991;34(7):799-807.
42. Polzer K, Schett G, Zwerina J. The lonely death: Chondrocyte apoptosis in TNF-induced arthritis: Brief Definition Report. Autoimmunity. 2007;40(4):333-6.
43. Kim HA, Song YW. Apoptotic chondrocyte death in rheumatoid arthritis. Arthritis Rheum. 1999;42(7):1528-37.

44. Goldring SR, Gravallese EM. Pathogenesis of bone erosions in rheumatoid arthritis. Curr Opin Rheumatol. 2000;12(3):195-9.
45. Pearson CM. Experimental joint disease: Observations on adjuvant-induced arthritis. J Chronic Dis. 1963;16(8):863-74.
46. Bizarro A. On sesamoid and supernumerary bones of the limbs. J Anat. 1921;55(Pt 4):256.
47. Doherty AH, Lowder EM, Jacquet RD, Landis WJ. Murine metapodophalangeal sesamoid bones: Morphology and potential means of mineralization underlying function. Anat Rec. 2010;293(5):775-85.
48. Resnick D, Niwayama G, Feingold ML. The Sesamoid Bones of the Hands and Feet: Participators in Arthritis 1. Radiology. 1977;123(1):57-62.
49. Lee DM, Friend DS, Gurish MF, Benoist C, Mathis D, Brenner MB. Mast cells: a cellular link between autoantibodies and inflammatory arthritis. Science. 2002;297(5587):1689-92.
50. Pastoureau P, Hunziker EB, Pelletier J-P. Cartilage, bone and synovial histomorphometry in animal models of osteoarthritis. Osteoarthritis Cartilage. 2010;18:S106-S12.
51. Barnabe C, Buie H, Kan M, Szabo E, Barr SG, Martin L, et al. Reproducible metacarpal joint space width measurements using 3D analysis of images acquired with high-resolution peripheral quantitative computed tomography. Med Eng Phys. 2013;35(10):1540-4.
52. Gundersen Ha, Østerby R. Optimizing sampling efficiency of stereological studies in biology: or 'Do more less well!'. J Microsc. 1981;121(1):65-73.